ORIGINAL ARTICLE

Consequences of Two Different Amino-Acid Substitutions at the Same Codon in *KRT14* Indicate Definitive Roles of Structural Distortion in Epidermolysis Bullosa Simplex Pathogenesis

Ken Natsuga[1], Wataru Nishie[1], Brian J. Smith[2,3], Satoru Shinkuma[1], Thomasin A. Smith[4], David A.D. Parry[4,5], Naoki Oiso[6], Akira Kawada[6], Kozo Yoneda[7], Masashi Akiyama[1,8] and Hiroshi Shimizu[1]

Numerous inherited diseases develop due to missense mutations, leading to an amino-acid substitution. Whether an amino-acid change is pathogenic depends on the level of deleterious effects caused by the amino-acid alteration. We show an example of different structural and phenotypic consequences caused by two individual amino-acid changes at the same position. Epidermolysis bullosa simplex (EBS) is a genodermatosis resulting from *KRT5* or *KRT14* mutations. Mutation analysis of an EBS family revealed that affected individuals were heterozygous for a, to our knowledge, previously unreported mutation of c.1237G>C (p.Ala413Pro) in *KRT14*. Interestingly, 2 of 100 unrelated normal controls were heterozygous, and 1 of the 100 was homozygous for a different mutation in this position, c.1237G>A (p.Ala413Thr). *In silico* modeling of the protein demonstrated deleterious structural effects from proline substitution but not from threonine substitution. *In vitro* transfection studies revealed a significantly larger number of keratin-clumped cells in HaCaT cells transfected with mutant *KRT14* complementary DNA (cDNA) harboring p.Ala413Pro than those transfected with wild-type *KRT14* cDNA or mutant *KRT14* cDNA harboring p.Ala413Thr. These results show that changes in two distinct amino acids at a locus are destined to elicit different phenotypes due to the degree of structural distortion resulting from the amino-acid alterations.

INTRODUCTION

Keratins are the largest group of intermediate filament proteins, which are expressed in epithelial cells (Schweizer *et al.*, 2006). The prominent intermediate filaments consist of keratins K1–K20, which are further classified into types I (K9–K20) and II (K1–K8). Type I and II keratins form non-covalent type I/II keratin heteropolymers (Moll *et al.*, 1982).

Unique keratin expression serves as specific markers that characterize different epithelial cell types. Of the many kinds of epithelial cells that exist, basal epidermal keratinocytes preferentially express K5/K14 heteropolymers (Moll *et al.*, 1982; Nelson and Sun, 1983). These, in turn, form predominantly heterodimers *in vivo* (Coulombe and Fuchs, 1990; Hatzfeld and Weber, 1990; Steinert, 1990), with chains parallel to one another and in axial register (Conway and Parry, 1990; Steinert *et al.*, 1993).

Epidermolysis bullosa (EB) comprises a group of heterogeneous disorders in which congenital skin fragility leads to dermal–epidermal junction separation. EB has been subdivided into three major groups (EB simplex, junctional EB, and dystrophic EB) and one minor subtype (Kindler syndrome) based on the level of blister formation (Fine *et al.*, 2008). So far, mutations in 14 different genes have been identified as underlying EB subtypes (Fine *et al.*, 2008; Groves *et al.*, 2010). Among them, mutations in either the *KRT5* or *KRT14* gene, which encodes K5 and K14, respectively, lead to EB simplex (EBS) (Coulombe *et al.*, 1991; Lane *et al.*, 1992; Yasukawa *et al.*, 2006). According to the clinical severity of blister formation, EBS can be further subdivided into three major subtypes (Fine *et al.*, 2008). The mildest variant is ''EBS, localized'' (EBS-loc), with blistering confined to the

[1]*Department of Dermatology, Hokkaido University Graduate School of Medicine, Sapporo, Japan;* [2]*Walter and Eliza Hall Institute of Medical Research, Parkville, Victoria, Australia;* [3]*Department of Medical Biology, University of Melbourne, Parkville, Victoria, Australia;* [4]*Institute of Fundamental Sciences, Massey University, Palmerston North, New Zealand;* [5]*Riddet Institute, Massey University, Palmerston North, New Zealand;* [6]*Department of Dermatology, Kinki University Faculty of Medicine, Osaka, Japan;* [7]*Department of Dermatology, Kagawa University Faculty of Medicine, Kagawa, Japan and* [8]*Department of Dermatology, Nagoya University Graduate School of Medicine, Nagoya, Japan*

Correspondence: Ken Natsuga, Department of Dermatology, Hokkaido University Graduate School of Medicine, North 15 West 7, Sapporo 060-8638, Japan. E-mail: natsuga@med.hokudai.ac.jp

hands and feet; the more moderate variant is ''EBS, other generalized'' (EBS-gen-non-DM), with generalized blister formation; and the most severe variant is Dowling–Meara type (EBS-DM), which is characterized by severe herpetiform blistering (Fine *et al.*, 2008; Coulombe *et al.*, 2009).

In this study, we identified a, to our knowledge, previously unreported missense mutation in *KRT14* from a family with EBS-loc. We also detected a different nucleotide substitution at the same position in *KRT14* in normal control individuals. To clarify whether each nucleotide substitution is pathogenic, we used molecular modeling to predict the effect on the structure that results from a single amino-acid change, and we examined cultured cells transfected either with wild-type or with mutated *KRT14* complementary DNA (cDNA). Here, we show that two kinds of amino-acid changes at the same position of *KRT14* lead to totally different cell function *in vitro* and phenotypes *in vivo*.

RESULTS

Case description

The proband was a 10-year-old male with blistering on his soles (Figure 1a). Blisters on his hands and feet were observed during infancy. New blisters tended to emerge more in the summer. Nail deformity was also noted (Figure 1b). Ultra-structural features of skin specimens from the proband revealed many vacuoles scattered between the nucleus and basal lamina in the basal keratinocytes (Figure 1c). His family had several affected members (Figure 1d).

Detection of a novel *KRT14* mutation in a family with EBS and another nucleotide substitution at the same position of *KRT14* in normal controls

Direct sequencing of the *KRT5/KRT14* gene revealed that the proband (III-2, Figure 1d) was heterozygous for the, to our knowledge, previously unreported mutation of c.1237G>C transversion (p.Ala413Pro) in the helix termination motif of *KRT14* (Figure 2a). No other mutations were detected in any of the exons or exon–intron boundaries of *KRT5* and *KRT14*.
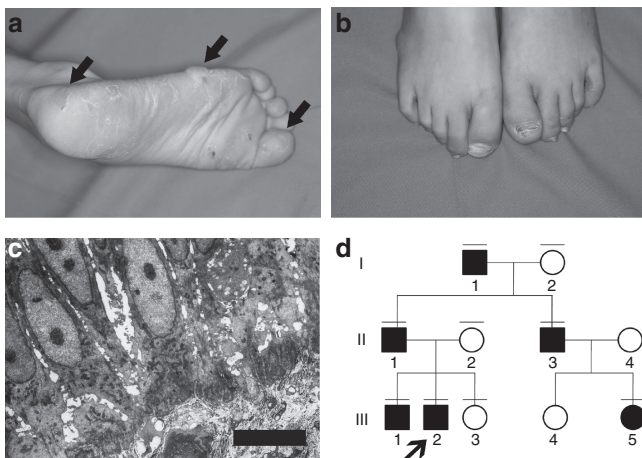
Figure 1. Clinical and ultrastructural features of a family with epidermolysis bullosa simplex. (**a**) Blisters and erosions are seen in the proband's right sole (arrows). (**b**) Toenail deformities are observed in the proband. (**c**) Ultrastructural features of the proband's lesional skin sample show basal cell cytolysis (bar = 5 μm). No apparent keratin clumps are seen. (**d**) Pedigree of the proband's family. Affected individuals are indicated by black fill. The proband is indicated by an arrow.
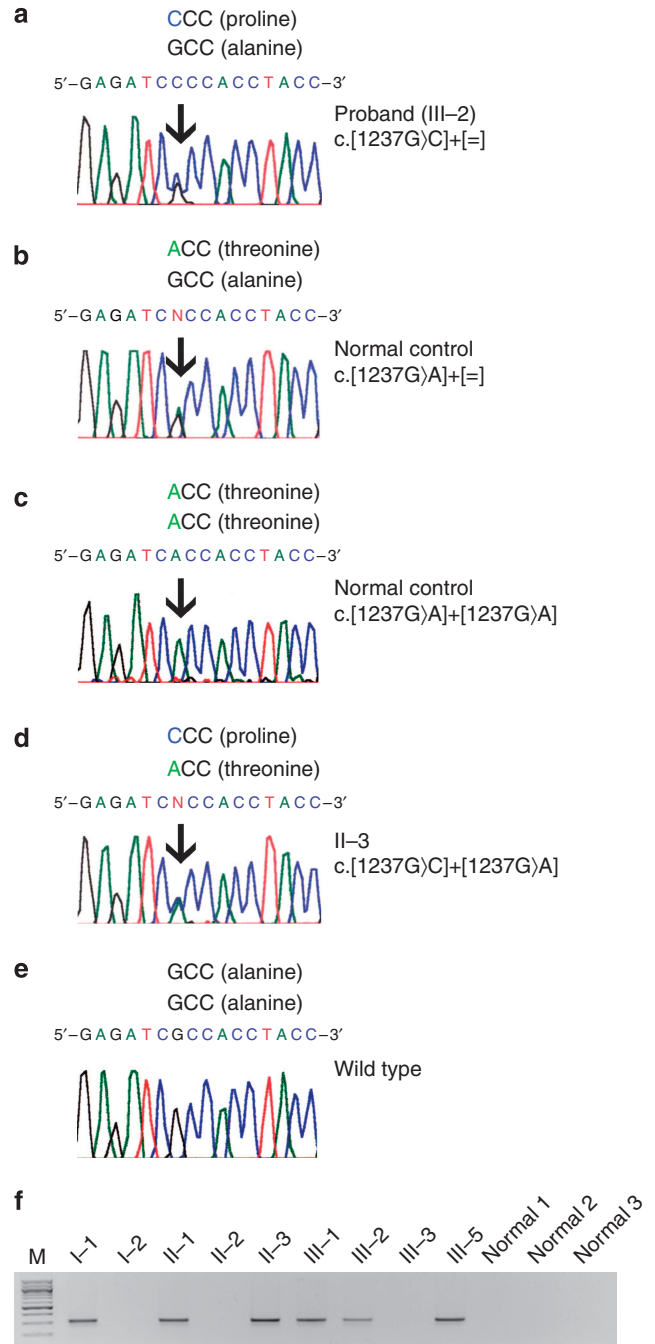
Figure 2. *KRT14* mutation analysis. (**a**) The proband (III-2) is heterozygous for c.1237G>C (p.Ala413Pro) in *KRT14* (an arrow). (**b**) In all, 2 out of 100 normal controls are heterozygous for c.1237G>A (p.Ala413Thr; an arrow). (**c**) Similarly, 1 out of 100 normal controls is homozygous for c.1237G>A (p.Ala413Thr; an arrow). (**d**) The proband's uncle (II-3) is compound heterozygous for c.1237G>C (p.Ala413Pro) and c.1237G>A (p.Ala413Thr; an arrow). (**e**) The wild-type sequence. (**f**) Mutant allele–specific amplification shows that affected family members (Figure 1d) harbor c.1237G>C (p.Ala413Pro).

Affected family members were also heterozygous for the same mutation in *KRT14* (I-1, II-1, II-3, III-1, and III-5; Figure 1d), and unaffected family members did not have that mutation (I-2, II-2, and III-3; Figure 1d). Mutant allele-specific amplification analysis demonstrated that a 300-bp fragment derived from the mutant allele was amplified from the genomic DNA of affected family members (Figures 1d and 2f). This mutation was not found in 200 normal unrelated alleles (100 Japanese individuals) by direct sequencing. Unexpectedly, 2 of the 100 normal Japanese controls were heterozygous for c.1237G>A transition (p.Ala413Thr) in *KRT14* (Figure 2b), and 1 of the 100 normal controls was homozygous for the same nucleotide transition (Figure 2c). These three individuals with the c.1237G>A transition (p.Ala413Thr) in *KRT14* had no history of skin fragility or nail dystrophy. Interestingly, the proband's unaffected grandmother (I-2) and affected uncle (II-3) were also heterozygous for the c.1237G>A transition (p.Ala413Thr) in *KRT14*. The proband's affected uncle (II-3) was compound heterozygous for p.Ala413Thr and p.Ala413Pro (Figure 2d). However, his clinical manifestations were similar to those of the other affected family members. The proband's unaffected cousin (III-4) is expected to be heterozygous for p.Ala413Thr—mutation analysis could not be performed without her consent.

Molecular dynamics predicts the deleterious structural change resulting from p.Ala413Pro substitution in keratin 14 but not from p.Ala413Thr

An initial structure of the native K5/K14 heterodimer and the p.Ala413Thr and p.Ala413Pro mutants, representing the C-terminal 35 residues of each chain, was generated by comparative modeling. The first 29 residues of each chain form a classical coiled coil in which generally hydrophobic residues occupy the heptad-repeat positions "*a*" and "*d*" (Figure 3a), a lysine at position 405 in K14 and 460 in K5,

conserved among human intermediate filament proteins (Strelkov *et al.*, 2002), interact with each other through the hydrophobic portion of their side chains.

The structure of the native K5/K14 and the two mutants were subjected to molecular dynamics (MD) simulations to explore the structural stability. The secondary structure content in each of the chains throughout the MD simulations is presented in Figure 3b–d—in this figure, α-helix conformation is represented in blue. In this native heterodimer (Figure 3b), the α-helix content remains essentially unchanged throughout the simulation—both peptides maintain helical geometry across the coiled-coil domains (residues 449–474 in K5 and 394–419 in K14). At the C termini of K5 and K14, a stable bend (green), flanked on the N-terminal side by a stable short turn (yellow), is observed. In K5, a short 3_{10} helix (gray) forms after ∼16 nanoseconds and is stable for the remainder of the simulation. Thus, the structure, and particularly the secondary structure conformation, remains constant throughout the simulation in the native complex.

The p.Ala413Thr mutation introduces a slight instability in the helix at the site of the mutation (black triangle), represented by an infrequent change in conformation to "turn" during the simulation (shown in yellow; Figure 3c). However, the overall α-helix content in this mutant is very similar to that observed for the native (Figure 3b). In contrast, in the p.Ala413Pro, peptide predominantly adopts a non-helical conformation at the position of the mutation throughout the simulation (Figure 3d). This change in conformation is also associated with additional instability (turn and coil conformation) in the helical conformation of residues C-terminal of the mutation site in both the K5 and K14 peptides (Figure 3d). Thus, the p.Ala413Thr mutation introduces a slight instability into the structure of the complex, whereas the p.Ala413Pro mutation causes significant disruption to the secondary structure in the C-terminal region of both peptides.
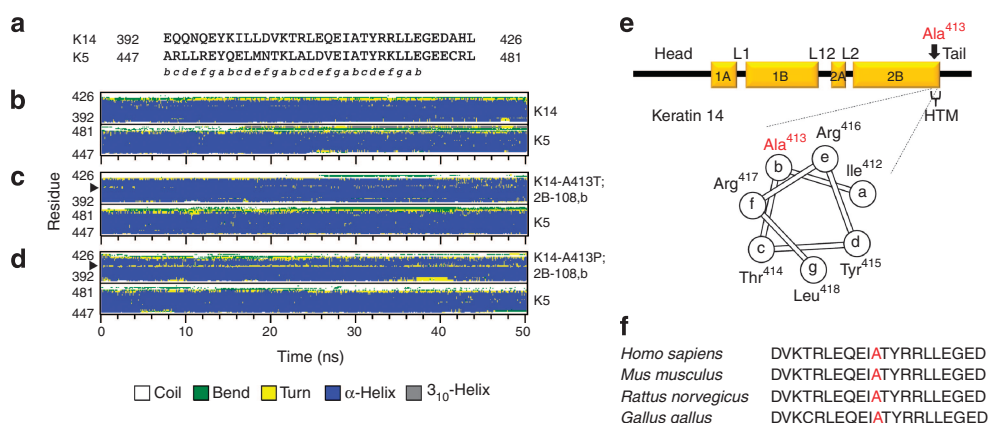

Figure 3. Molecular dynamics (MD) of the keratin heterodimer. (**a**) Sequences of the keratin helix motif and the heptad-repeat positions in K5 and K14. (**b–d**) MD simulations. The changes in secondary structure due to an amino-acid substitution were visualized through the MD. These simulations were each run for 50.0 nanoseconds. Blue indicates the α-helix. The native (**b**) and p.Ala413Thr (**c**) peptides retain α-helix geometry (blue colored) throughout the simulation. In contrast, increased instability in the α-helix was observed in the p.Ala413Pro-mutant peptide (**d**) bound with K5, which is indicated by the appearance of yellow-colored turn motif (arrowheads). In the p.Ala413Pro peptide (**d**), the helical geometry at the C terminus of both K14 and K5 is substantially compromised throughout the simulation—K5 is unstructured (coil geometry), and K14 alternates between coil, bends, and turns geometries. (**e**) A schematic diagram of K14 structure. Note that Ala[413] is located at the helix termination motif (HTM) of the keratin molecule. Ala[413] corresponds to position "*b*" of the heptad repeat (*abcdefg*) and is conserved among keratin polypeptides. (**f**) K14 amino-acid sequence alignment shows the level of conservation in diverse species of the amino acid Ala[413] (red characters).

An alanine to proline substitution at the 413 locus of KRT14 protein disrupts the KIF network in HaCaT cells, whereas alanine to threonine does not

We examined whether the clinical heterogeneity between individuals with wild-type, p.Ala413Thr, and p.Ala413Pro mutations in *KRT14* could be demonstrated in a cell culture system. Three mammalian expression vectors containing the wild-type *KRT14* cDNA (K14WT), the mutated *KRT14* cDNA correspondent with the p.Ala413Thr substitution (K14A413T), and the p.Ala413Pro substitution (K14A413P) were transiently transfected into HaCaT cells. Detection of K14 was performed by probing the V5 epitope tag. Immunoblot analysis confirmed that each construct was successfully transferred into the HaCaT cells (Figure 4a).
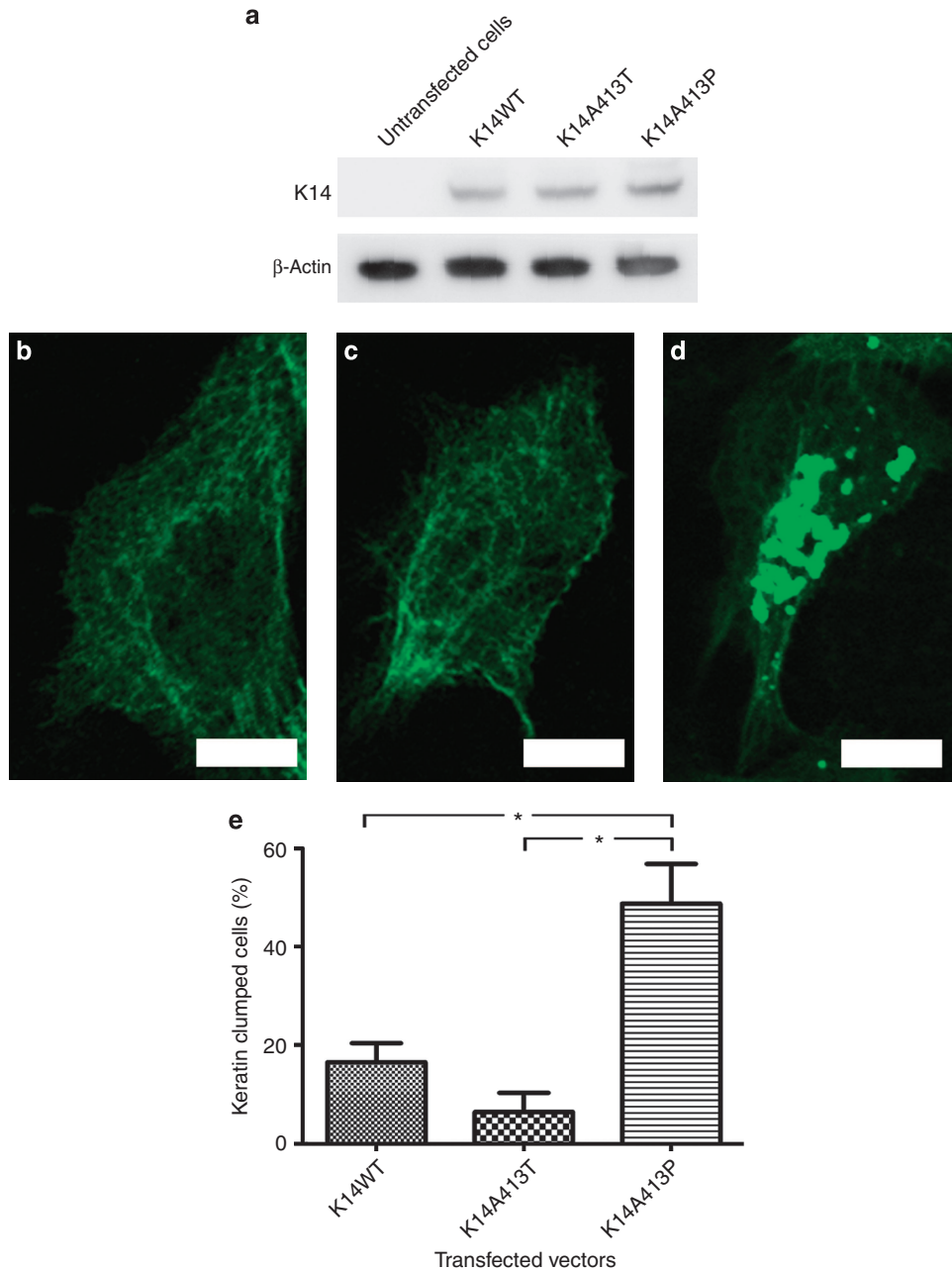
Figure 4. *In vitro* assay using HaCaT cells transfected with mutated *KRT14* complementary DNA (cDNA). (a) Immunoblot analysis reveals that HaCaT cells transfected with either wild-type (K14WT) or mutated *KRT14* cDNA (K14A413T and K14A413P) express V5-tagged K14 molecules. Equal protein loading was confirmed by reprobing with AC15 (anti-β-actin antibody). HaCaT cells transfected with K14WT (b), K14A413T (c), or K14A413P (d; bar = 5 μm). To visualize the transfected gene product, cells were stained with FITC-conjugated anti-V5 antibody. Cells transfected with K14WT and K14A413T have a normal keratin filament network (b, c), whereas significantly more cells transfected with K14A413P exhibit small ball-like clump formation (d). (e) The percentage of cells showing keratin aggregate formation among transfected cells is compared. There are significantly more clumps observed in the K14A413P-transfected cells (49 ± 8%) than in those transfected with either K14WT (17 ± 3%) or K14A413T (6 ± 4%). Each value shown represents the mean ± SEM of 10 individual samples. The statistical significance of the differences between groups is assessed by one-way analysis of variance, followed by Tukey's test (*$P < 0.05$).

Transfection efficiency was up to 50% as judged from the immunofluorescence of the V5 epitope tag in transfected cells. The cells transfected with either K14WT or K14A413T showed fine bundles of keratin filaments extending throughout the cytoplasm without disturbing the cells' morphology (Figure 4b and c), whereas cells transfected with K14A413P exhibited small ball-like filament aggregates, indicating a disruption in the keratin network (Figure 4d). The percentage of the transfected cells harboring keratin clumping in each transfection assay was as follows: K14WT (mean, 17%), K14A413T (6%), and K14A413P (49%; Figure 4e). Statistical analysis showed that significantly more clumped cells were observed in HaCaT cells transfected with K14A413P than in those transfected with K14WT or K14A413T ($P<0.05$; Figure 4e).

Although not statistically significant ($P>0.05$), fewer keratin-clumped cells were observed in HaCaT cells transfected with K14A413T than those transfected with K14WT (Figure 4e). To clarify whether p.Ala413Thr mutation has a protective effect on keratin aggregation, three different transfections using HaCaT cells were performed, including K14A413P alone, a combination of equal amounts of K14A413P and K14A413T (K14A413P/K14A413T), and a combination of equal amounts of K14A413P and K14WT (K14A413P/K14WT). The percentage of the transfected cells harboring keratin clumping in each transfection assay was as follows: K14A413P (mean, 42%), K14A413P/K14A413T (32%), and K14A413P/K14WT (30%; Supplementary Figure S1 online). The differences in the percentage of keratin-clumped cells between K14A413P/K14A413T and K14A413P/K14WT were not statistically significant ($P>0.05$), indicating that the p.Ala413Thr mutation is unlikely to have a protective effect on keratin aggregation compared with the wild-type sequence.

We further performed three different transfections (K14WT, K14A413T, and K14A413P) into HeLa cells, in which endogenous K5 and K14 were not expressed but K8 was present as a potential partner of recombinant K14 (Hatzfeld and Franke, 1985; Albers and Fuchs, 1987). The percentage of the transfected cells harboring keratin aggregation in each transfection assay was as follows: K14WT (mean, 14%), K14A413T (10%), and K14A413P (77%; Supplementary Figure S2 online). Statistical analysis showed that significantly more clumped cells were observed in HeLa cells transfected with K14A413P than in those transfected with K14WT or K14A413T ($P<0.05$; Supplementary Figure S2 online), confirming the deleterious effect of p.Ala413Pro mutation in K14 on keratin filament network. In contrast, no keratin clumping was observed in normal human epidermal keratinocytes (NHEKs) transfected with any of the three plasmids (K14WT, K14A413T, and K14A413P; Supplementary Figure S3 online).

DISCUSSION
A single-nucleotide change in the protein-coding region that leads to an amino-acid substitution can be assigned either as a non-synonymous-coding single-nucleotide polymorphism or as a missense mutation. Numerous single-gene diseases

have been attributed to missense mutations. However, it is sometimes difficult to demonstrate the effects of an amino-acid substitution on protein function and disease phenotype (Thusberg and Vihinen, 2009); it has been recently shown that the p.Met119Thr and p.Met119Val mutations in K14 result in EBS-DM and EBS-gen-non-DM, respectively (Cummins et al., 2001). Our study provides a good model to study the pathogenicity of a single amino-acid substitution, as replacement of Ala[413] in K14 with proline results in an EBS family, whereas replacement with threonine results in normal controls.

Ala[413] is located in the helix termination motif of K14 and corresponds to position ''b'' of the heptad repeat (*abcdefg*) that is conserved among keratin polypeptides (Figure 3e), where ''a'' and ''d'' are usually non-polar amino acids and the others are polar or charged. Ala[413] is highly conserved among species (Figure 3f).

Proline lacks an amide hydrogen atom and is unable to form a hydrogen bond with the carbonyl oxygen atom of the four amide residues N-terminal of it in an α-helix; thus, proline residues act as α-helix disruptors (although the stability of α-helices harboring a proline may be environment specific (Li et al., 1996)). Previous reports using crystal X-ray analysis showed marked structural perturbations by proline residues in polypeptides (MacArthur and Thornton, 1991). Keratin has a conserved structure with helix motifs, and proline substitutions in these motifs have been reported to cause marked structural perturbations (Letai et al., 1992). As for EBS, proline substitutions in K5/K14 have been described in 34 cases in the Human Intermediate Filament Database (http://www.interfil.org/; Szeverenyi et al., 2008), although no non-synonymous-coding single-nucleotide polymorphisms have been detected in the database that cause proline substitutions. Clinical manifestations in EBS with proline substitutions vary between the localized and Dowling–Meara types, although proline substitutions in helix motifs tend to lead to EBS-DM, and those substitutions in domains outside helix motifs are more often observed in EBS-gen-non-DM.

A Taiwanese patient with EBS-loc has been described as heterozygous for p.Ala413Thr in K14 (Chao et al., 2002). However, p.Ala413Thr was recently found in 6 of 112 alleles in normal Japanese individuals (Hattori et al., 2006). Our study confirmed the presence of normal control individuals who are heterozygous for p.Ala413Thr (Figure 2b). Furthermore, a single normal control was homozygous for p.Ala413Thr (Figure 2c), which lowers the possibility of pathogenic effects from threonine substitution at this amino acid. Threonine and alanine substitute for one another on a frequency commensurate with their occurrence in structured proteins (Henikoff and Henikoff, 1992). Thus, structurally they can be considered interchangeable. Proline, on the other hand, is seldom observed to substitute for any residue, including alanine, highlighting its unique structural characteristics. Our *in vitro* study using HaCaT cells confirmed that it is not threonine substitution but proline substitution that causes keratin aggregation. Nevertheless, it is possible that p.Ala413Thr is a phenotypical mutation in

certain environmental conditions, as many contributing factors including temperature, trauma, and location of blister formation can affect the development of blistering phenotypes (Coulombe *et al.*, 2009).

Modeling of K5/K14 mutations in coiled-coil structures provides evidence that a correlation exists between the clinical severity of EBS and the degree of structural distortion caused by the underlying amino-acid change (Smith *et al.*, 2004). Our study has also demonstrated that MD simulations of keratin mutations accurately correlate with the pathogenicity of an amino-acid substitution.

As HaCaT cells are not normal keratinocytes, their keratin expression level is different from that of NHEK (Boukamp *et al.*, 1988). No keratin clumping was seen in NHEK transfected with any of K14WT, K14A413T, or K14A413P (Supplementary Figure S3 online). This result indicates that either overexpressed recombinant K14 is not enough to disrupt keratin network in NHEK due to a much higher expression of endogenous K14 in NHEK than in HaCaT cells (Sorensen *et al.*, 2003). On the other hand, the balance of keratin network may be substantially altered when recombinant K14 is overexpressed in HaCaT cells, in which endogenous K14 is reduced compared with NHEK (Sorensen *et al.*, 2003). The absence of keratin aggregation in the proband's skin keratinocytes (Figure 1c), compared with what was observed in HaCaT cells transfected with K14A413P, may reflect the greater effect of K14 mutant introduction in HaCaT cells compared with NHEK.

In summary, this study gives insight into consequences of two different amino-acid substitutions at the same codon. The biological effects of one amino-acid substitution are hard to predict. *In silico* and *in vitro* analyses are useful for confirming the pathogenicity of missense mutations.

MATERIALS AND METHODS
Mutation analysis
Genomic DNA extracted from peripheral blood was used as a template for PCR amplification. The *KRT5* and *KRT14* genes were amplified by methods previously described (Stephens *et al.*, 1997; Hut *et al.*, 2000). DNA sequencing of the PCR products was carried out with an ABI 3100 sequencer (PerkinElmer Life Sciences-ABI, Foster City, CA). The mutation nomenclature follows published mutation nomenclature guidelines (http://www.hgvs.org/mutnomen) according to the reference sequence NM_000424.3 for *KRT5* and NM_000526.3 for *KRT14*, with $+1$ as the A of the ATG initiation codon.

Mutant allele-specific amplification analysis
To verify the mutation, mutant allele-specific amplification analysis was performed with mutant allele-specific primers carrying the substitution of two bases at the 3′-end mutant allele-specific primers (Linard *et al.*, 2002; Sapio *et al.*, 2006): forward, 5′-ACGCG GCTGGAGCAGGAGATTC-3′ and reverse, 5′-GACAGCACTAGAGC TCAGCC-3′. PCR conditions were as follows: 94°C for 5 minutes, followed by 30 cycles of 94°C for 30 seconds, 65°C for 30 seconds, 72°C for 30 seconds, and extension at 72°C for 7 minutes.

Plasmid construction
cDNA containing the entire coding region of *KRT14* (K14WT) subcloned into the pcDNA 3.1/V5-His vector (Invitrogen, Carlsbad, CA) was employed (Yoneda *et al.*, 2004). The point-mutated *KRT14* cDNAs corresponding to the p.Ala413Pro (K14A413P) and p.Ala1237Thr (K14A413T) mutations were generated with the use of the GeneTailor Site-Directed Mutagenesis System (Invitrogen). Sense primers used for the PCR reactions to generate the K14A413P and the K14A413T fragments were 5′-CGCGGCTGGAGCAGGAGA TC**c**CCACCTACCGC-3′ and 5′-CGCGGCTGGAGCAGGAGATC**a**CCA CCTACCGC-3′, respectively (lower-case letters in bold denote mutations introduced). The anti-sense primer 5′-GATCTCCTGCTCCA GCCGCGTCTTCACGTC-3′ was used to generate both of the mutant *KRT14* cDNAs.

Molecular modeling
The structure of segment 2B in human vimentin (PDB 1GK6) (Herrmann *et al.*, 2000; Strelkov *et al.*, 2002, 2004) was used as a template in comparative modeling of the K5/K14 heterodimer and the two mutations (K14-A413P and K14-A413T: 2B-108,*b*) using the Modeller (9v7) program (Fiser and Sali, 2003). The nomenclature K14-A413P: 2B-108,*b* specifies residue 413 in chain K14, its position 108 within segment 2B, and its position *b* within the heptad repeat. From 25 models of each heterodimer, the structure with the lowest Modeller Objective function was subjected to MD simulation.

MD simulations using the GROMACS (v4.0) package of programs (Hess *et al.*, 2008) were performed using the OPLS-aa force field (Jorgensen and Tirado-Rives, 1988). Ionizable residues were assumed to be in their charged state, whereas the amine and carboxyl termini were assumed to be in their neutral form. Each molecule was solvated in a $75 \times 75 \times 75$ Å^3 water box; sodium and chloride ions were added to neutralize the system and provide a final ionic strength of 0.154 M. Protein and water (with ions) were coupled separately to a thermal bath at 300 K using velocity rescaling (Bussi *et al.*, 2007) applied with a coupling time of 0.1 ps, whereas the pressure was coupled to an isotropic barostat using a time constant of 1 ps and compressibility of 4.5×10^{-5} bar^{-1}. All simulations were performed with a single non-bonded cutoff of 10 Å and applying a neighbour-list update frequency of 10 steps (20 fs). The particle-mesh Ewald method was used to account for long-range electrostatics (Essman *et al.*, 1995), applying a grid width of 1.2 Å, and a fourth-order spline interpolation. Bond lengths were constrained using the LINCS algorithm (Hess, 2008; Hess *et al.*, 2008). All simulations consisted of an initial minimization of water molecules, followed by 100 ps of MD with the protein restrained. Following positional restraints of MD, all restraints on the protein were removed and MD continued for a further 50 ns. Coordinates were archived throughout the simulation at 100-ps intervals.

Cell culture and plasmid transfection
HaCaT-immortalized keratinocytes and HeLa cells were maintained in DMEM (GIBCO, Grand Island, NY) supplemented with 10% (v/v) fetal bovine serum. NHEKs from neonatal foreskin (Lonza, Allendale, NJ) were cultured in keratinocyte growth medium (Lonza). Three different transfections (K14WT, K14A413P, and K14A413T) into HaCaT cells or HeLa cells (2 μg of plasmid in six-well dishes) were performed using Lipofectamine LTX (Invitrogen) according

to the manufacturer's instructions. Three different plasmids (K14WT, K14A413P, and K14A413T) were transfected, respectively, into NHEK (5 µg of plasmid in six-well dishes) with electroporation using Amaxa Nucleofector apparatus (Amaxa, Cologne, Germany). Also, three different transfections into HaCaT cells, including K14A413P alone (2 µg of plasmid in six-well dishes), a combination of equal amounts of K14A413P (1 µg) and K14WT (1 µg; K14A413P/K14WT), and a combination of equal amounts of K14A413P (1 µg) and K14A413T (1 µg; K14A413P/K14A413T) were performed using Lipofectamine LTX (Invitrogen).

Immunoblot analysis

At 24 hours after transfection, HaCaT cells were lysed in Laemmli buffer (consisting of 62.5 mM Tris-HCl (pH 6.8), 3% SDS, and 5% mercaptoethanol) on ice for 10 minutes, cell debris was removed by centrifugation at 14,000 rpm for 5 minutes, and supernatant was collected. Supernatants were electrophoresed on a NuPAGE 4–12% bis-Tris gel (Invitrogen) and transferred to a polyvinylidene difluoride membrane. The membrane was incubated with horseradish perox-idase-conjugated anti-V5 antibody (Invitrogen) for 1 hour at room temperature, and the blots were detected using the ECL Plus Detection Kit (GE Healthcare, Waukesha, WI).

Confocal laser analysis

At 24 hours after transfection, the cells were washed with phosphate-buffered saline and fixed with methanol. A FITC-conjugated anti-V5 antibody (Invitrogen) was used to detect transfected cells. All cells were observed using a confocal laser-scanning microscope (Olympus Fluoview FV300, Tokyo, Japan). The cells with keratin aggregates were counted in five different areas, two from each experimental replicate (a mean of 42 cells from each replicate), as described previously (Yasukawa *et al.*, 2002), and the results obtained from the 10 counts were expressed as the mean ± SEM.

Ethics

The medical ethics committee of Hokkaido University Graduate School of Medicine approved all studies. The study was conducted according to the Declaration of Helsinki Principles. Participants or their legal guardians gave written informed consent.

SUPPLEMENTARY MATERIAL
Supplementary material is linked to the online version of the paper at http://www.nature.com/jid

REFERENCES
Albers K, Fuchs E (1987) The expression of mutant epidermal keratin cDNAs transfected in simple epithelial and squamous cell carcinoma lines. *J Cell Biol* 105:791–806

Boukamp P, Petrussevska RT, Breitkreutz D, Hornung J, Markham A, Fusenig NE (1988) Normal keratinization in a spontaneously immorta-lized aneuploid human keratinocyte cell line. *J Cell Biol* 106:761–71

Bussi G, Donadio D, Parrinello M (2007) Canonical sampling through velocity rescaling. *J Chem Phys* 126:014101

Chao SC, Yang MH, Lee SF (2002) Novel KRT14 mutation in a Taiwanese patient with epidermolysis bullosa simplex (Kobner type). *J Formos Med Assoc* 101:287–90

Conway JF, Parry DAD (1990) Structural features in the heptad substructure and longer range repeats of two-stranded alpha-fibrous proteins. *Int J Biol Macromol* 12:328–34

Coulombe PA, Fuchs E (1990) Elucidating the early stages of keratin filament assembly. *J Cell Biol* 111:153–69

Coulombe PA, Hutton ME, Letai A, Hebert A, Paller AS, Fuchs E (1991) Point mutations in human keratin 14 genes of epidermolysis bullosa simplex patients: genetic and functional analyses. *Cell* 66:1301–11

Coulombe PA, Kerns ML, Fuchs E (2009) Epidermolysis bullosa simplex: a paradigm for disorders of tissue fragility. *J Clin Invest* 119:1784–93

Cummins RE, Klingberg S, Wesley J, Rogers M, Zhao Y, Murrell DF (2001) Keratin 14 point mutations at codon 119 of helix 1A resulting in different epidermolysis bullosa simplex phenotypes. *J Invest Dermatol* 117:1103–7

Essman U, Perela L, Berkowitz ML, Darden T, Lee H, Pedersen LG (1995) A smooth particle mesh Ewald method. *J Chem Phys* 103:8577–92

Fine JD, Eady RA, Bauer EA, Bauer JW, Bruckner-Tuderman L, Heagerty A *et al.* (2008) The classification of inherited epidermolysis bullosa (EB): Report of the Third International Consensus Meeting on Diagnosis and Classification of EB. *J Am Acad Dermatol* 58:931–50

Fiser A, Sali A (2003) Modeller: generation and refinement of homology-based protein structure models. *Methods Enzymol* 374:461–91

Groves RW, Liu L, Dopping-Hepenstal PJ, Markus HS, Lovell PA, Ozoemena L *et al.* (2010) A homozygous nonsense mutation within the *dystonin* gene coding for the coiled-coil domain of the epithelial isoform of BPAG1 underlies a new subtype of autosomal recessive epidermolysis bullosa simplex. *J Invest Dermatol* 130:1551–7

Hattori N, Komine M, Kaneko T, Shimazu K, Tsunemi Y, Koizumi M *et al.* (2006) A case of epidermolysis bullosa simplex with a newly found missense mutation and polymorphism in the highly conserved helix termination motif among type I keratins, which was previously reported as a pathogenic missense mutation. *Br J Dermatol* 155:1062–3

Hatzfeld M, Franke WW (1985) Pair formation and promiscuity of cytokeratins: formation *in vitro* of heterotypic complexes and inter-mediate-sized filaments by homologous and heterologous recombina-tions of purified polypeptides. *J Cell Biol* 101:1826–41

Hatzfeld M, Weber K (1990) The coiled coil of *in vitro* assembled keratin filaments is a heterodimer of type I and II keratins: use of site-specific mutagenesis and recombinant protein expression. *J Cell Biol* 110:1199–210

Henikoff S, Henikoff JG (1992) Amino acid substitution matrices from protein blocks. *Proc Natl Acad Sci USA* 89:10915–9

Herrmann H, Strelkov SV, Feja B, Rogers KR, Brettel M, Lustig A *et al.* (2000) The intermediate filament protein consensus motif of helix 2B: its atomic structure and contribution to assembly. *J Mol Biol* 298:817–32

Hess B (2008) P-LINCS: a parallel linear constraint solver for molecular simulation. *J Chem Theory Comput* 4:116–22

Hess B, Kutzner C, van der Spoel D, Lindahl E (2008) GROMACS 4: algorithms for highly efficient, load-balanced, and scalable molecular simulation. *J Chem Theory Comput* 4:435–47

Hut PH, v d Vlies P, Jonkman MF, Verlind E, Shimizu H, Buys CH *et al.* (2000) Exempting homologous pseudogene sequences from polymerase chain reaction amplification allows genomic keratin 14 hotspot mutation analysis. *J Invest Dermatol* 114:616–9

Jorgensen WL, Tirado-Rives J (1988) The OPLS potential functions for proteins. Energy minimizations for crystals of cyclic peptides of crambin. *J Am Chem Soc* 110:1657–66

Lane EB, Rugg EL, Navsaria H, Leigh IM, Heagerty AH, Ishida-Yamamoto A *et al.* (1992) A mutation in the conserved helix termination peptide of keratin 5 in hereditary skin blistering. *Nature* 356:244–6

Letai A, Coulombe PA, Fuchs E (1992) Do the ends justify the mean? Proline mutations at the ends of the keratin coiled-coil rod segment are more disruptive than internal mutations. *J Cell Biol* 116:1181–95

Li SC, Goto NK, Williams KA, Deber CM (1996) Alpha-helical, but not beta-sheet, propensity of proline is determined by peptide environment. *Proc Natl Acad Sci USA* 93:6676–81

Linard B, Bezieau S, Benlalam H, Labarriere N, Guilloux Y, Diez E *et al.* (2002) A ras-mutated peptide targeted by CTL infiltrating a human melanoma lesion. *J Immunol* 168:4802–8

MacArthur MW, Thornton JM (1991) Influence of proline residues on protein conformation. *J Mol Biol* 218:397–412

Moll R, Franke WW, Schiller DL, Geiger B, Krepler R (1982) The catalog of human cytokeratins: patterns of expression in normal epithelia, tumors and cultured cells. *Cell* 31:11–24

Nelson WG, Sun TT (1983) The 50- and 58-kdalton keratin classes as molecular markers for stratified squamous epithelia: cell culture studies. *J Cell Biol* 97:244–51

Sapio MR, Posca D, Troncone G, Pettinato G, Palombini L, Rossi G *et al.* (2006) Detection of BRAF mutation in thyroid papillary carcinomas by mutant allele-specific PCR amplification (MASA). *Eur J Endocrinol* 154:341–8

Schweizer J, Bowden PE, Coulombe PA, Langbein L, Lane EB, Magin TM *et al.* (2006) New consensus nomenclature for mammalian keratins. *J Cell Biol* 174:169–74

Smith TA, Steinert PM, Parry DAD (2004) Modeling effects of mutations in coiled-coil structures: case study using epidermolysis bullosa simplex mutations in segment 1a of K5/K14 intermediate filaments. *Proteins* 55:1043–52

Sorensen CB, Andresen BS, Jensen UB, Jensen TG, Jensen PK, Gregersen N *et al.* (2003) Functional testing of keratin 14 mutant proteins associated with the three major subtypes of epidermolysis bullosa simplex. *Exp Dermatol* 12:472–9

Steinert PM (1990) The two-chain coiled-coil molecule of native epidermal keratin intermediate filaments is a type I-type II heterodimer. *J Biol Chem* 265:8766–74

Steinert PM, Marekov LN, Parry DAD (1993) Conservation of the structure of keratin intermediate filaments: molecular mechanism by which different keratin molecules integrate into preexisting keratin intermediate filaments during differentiation. *Biochemistry* 32:10046–56

Stephens K, Ehrlich P, Weaver M, Le R, Spencer A, Sybert VP (1997) Primers for exon-specific amplification of the *KRT5* gene: identification of novel and recurrent mutations in epidermolysis bullosa simplex patients. *J Invest Dermatol* 108:349–53

Strelkov SV, Herrmann H, Geisler N, Wedig T, Zimbelmann R, Aebi U *et al.* (2002) Conserved segments 1A and 2B of the intermediate filament dimer: their atomic structures and role in filament assembly. *EMBO J* 21:1255–66

Strelkov SV, Schumacher J, Burkhard P, Aebi U, Herrmann H (2004) Crystal structure of the human lamin A coil 2B dimer: implications for the head-to-tail association of nuclear lamins. *J Mol Biol* 343:1067–80

Szeverenyi I, Cassidy AJ, Chung CW, Lee BT, Common JE, Ogg SC *et al.* (2008) The Human Intermediate Filament Database: comprehensive information on a gene family involved in many human diseases. *Hum Mutat* 29:351–60

Thusberg J, Vihinen M (2009) Pathogenic or not? And if so, then how? Studying the effects of missense mutations using bioinformatics methods. *Hum Mutat* 30:703–14

Yasukawa K, Sawamura D, Goto M, Nakamura H, Jung SY, Kim SC *et al.* (2006) Epidermolysis bullosa simplex in Japanese and Korean patients: genetic studies in 19 cases. *Br J Dermatol* 155:313–7

Yasukawa K, Sawamura D, McMillan JR, Nakamura H, Shimizu H (2002) Dominant and recessive compound heterozygous mutations in epidermolysis bullosa simplex demonstrate the role of the stutter region in keratin intermediate filament assembly. *J Biol Chem* 277:23670–4

Yoneda K, Furukawa T, Zheng YJ, Momoi T, Izawa I, Inagaki M *et al.* (2004) An autocrine/paracrine loop linking keratin 14 aggregates to tumor necrosis factor alpha-mediated cytotoxicity in a keratinocyte model of epidermolysis bullosa simplex. *J Biol Chem* 279:7296–303